

# **Optimizing micromechanical force detectors for measuring magnetization at high magnetic fields**

Jeremy Paster  
University of Florida  
July 30, 2008

## **Abstract**

MEMS devices prove to be advantageous in magnetometry. The magnetization of tiny particles can be determined when glued to the top plate of micromachined parallel plate capacitors. Magnetometer designs were tested for effectiveness and simulated using COMSOL Multiphysics. Presented here are details of fabrication, testing, and simulation of MEMS magnetometers.

## **I. Introduction**

Magnetization measurement is an essential tool in condensed matter physics. Konstantinos Ninios, under the direction of Professor Ho Bun Chan at the University of Florida, has been working with microelectromechanical systems (MEMS) to develop magnetometers. The purpose of his research is to develop a method for measuring the magnetic moment of tiny particles in pulsed and dc magnetic fields. Numerous techniques have already been developed. Some commonly used include the vibrating sample magnetometers (VSM) and the superconducting quantum interference devices (SQUID). The use of MEMS for magnetometry is advantageous over these methods. For instance, this method is applicable in both high fields and low temperatures, and it allows for the measurement of very small particles [1].

MEMS, true to their name, are microsystems which incorporate moving parts and electrical components [2]. The MEMS are designed in-house and fabricated by a commercial manufacturer, MEMSCAP, using integrated circuit technology. Moveable parts are fabricated in layers using photolithography and selective etching. The devices arrive as layers of polysilicon held stiff with sacrificial layers of silicon dioxide. Additional fabrication techniques (wet etching, wire bonding), as well as some calibration steps, are required to prepare the structures for magnetometry.

The magnetometer consists of a square conductive plate (typically  $500 \mu\text{m} \times 500 \mu\text{m} \times 3.5 \mu\text{m}$ ) suspended above a square fixed electrode of equal area. The top plate is suspended by springs on all four sides. Spring designs vary according to intent. As Fig. 1 demonstrates, the device resembles a parallel plate capacitor. We glue a magnetic particle to the center of the free plate. When a magnetic field  $H$  is applied, its gradient generates a force  $\vec{F}_m = \vec{m} \cdot \nabla \vec{H}$  on the magnetized particle where  $\vec{m}$  is the particle's magnetic moment. The magnetic force is balanced by the spring force  $F_s = kx$ . We can extract the magnetic force from the change in capacitance between the two plates, assuming we know the spring constant. Once we know the value of the magnetic force, we can derive the magnetic moment of the particle  $\vec{m} = \frac{\vec{F}}{|\nabla \vec{H}|}$  if we know the gradient of the magnetic field [1].

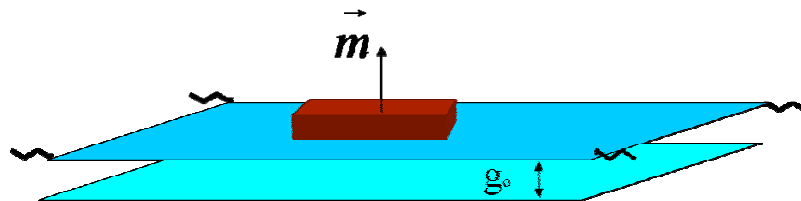


Fig. 1. Magnetic particle on suspended top plate [1].

This calculation assumes that the top plate remains flat and parallel to the electrode. However, with current designs this is not the case. The magnetic sample and hence the top plate experience a magnetic torque  $\vec{\tau}_m = \vec{m} \times \vec{H}$  due to the interaction of the moment  $\vec{m}$  with the magnetic field  $\vec{H}$ . For the prescribed method for magnetization derivation, this torque is indistinguishable from the magnetic force  $\vec{F}_m$  [1]. Additionally, the top plate has been found to deform under the given forces. This can be linked to compressive stress in the top plate, and boundary conditions where the spring is attached to the top plate. These problems prevent us from using the observed capacitance between the plates as an indicator of plate displacement. Consequently, magnetization measurements are not guaranteed to be accurate.

One purpose of this project was to prepare and test devices. In particular, we wanted to investigate a new spring design which reduced the response to torque by a factor of 10 [1]. In conjunction with experimentation, we incorporated computer simulation. I used COMSOL Multiphysics software to simulate properties of this new magnetometer design and optimize parameters to reduce plate deformation.

## **II. Device preparation**

The MEMS devices are fabricated by MEMSCAP using PolyMUMPs, a three-layer polysilicon surface micromachining process. Thin films of polysilicon, which make up the moveable components, are deposited in layers using low-pressure chemical vapor deposition (LPCVD). First, silicon nitride is deposited onto a silicon wafer as an electrical isolation layer. The bottom plate (electrode) is fabricated from a first layer of

polysilicon. Next, phosphosilicate glass (PSG) is deposited for a sacrificial layer. The top plate is comprised of the last two layers of polysilicon which are deposited onto the PSG.

At each instance of layer deposition, patterning ensues. Using photolithography and reactive ion etching (RIE), a particular layer is chiseled according to design specification (Fig. 2). A particular layer is patterned by first coating the surface with photoresist. The photoresist is exposed to UV light under the appropriate mask. The exposed photoresist is then cleared away, leaving the desired etch mask. RIE removes the underlying layer wherever it is not protected by the remaining photoresist. Once the underlying layer is patterned, the remaining photoresist can be removed [3].

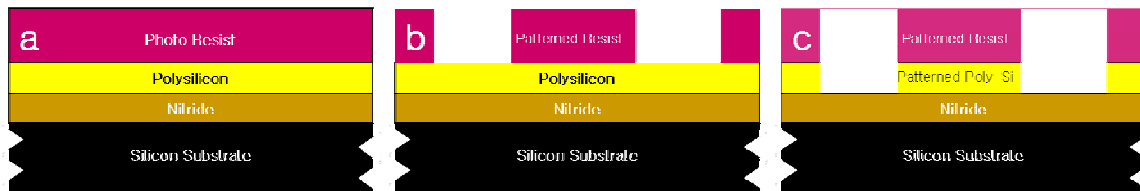


Fig. 2. (a) Photoresist is deposited, then (b) photoresist is patterned with UV light. (c) The underlying layer is patterned using RIE.

When we receive the devices from MEMSCAP, we must etch the sacrificial oxide layer to free the top plate. We use hydrofluoric acid (49%) as a wet isotropic etchant. The next step is to electrically connect the devices to the outside world. Magnetometer devices come on a small chip which can be secured to a lateral conducting package. Bonding pads are connected to the two plates via the polysilicon layers during the PolyMUMPs process. We wire bond these pads to the package to complete electrical preparation. Fig. 3 shows a device wired to a bonding package.

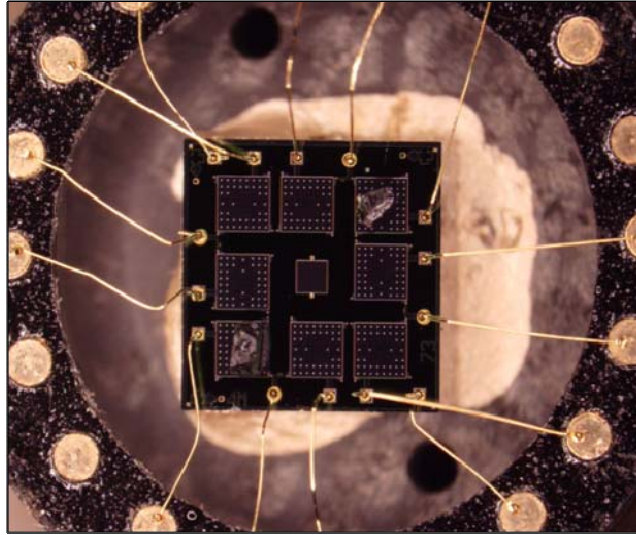


Fig. 3. Device wired to circular bonding package.

### III. Testing the device

#### A. Experiment setup

I considered three magnetometer designs. Each design varied further in spring size. A given chip included only devices of a particular design. In one design, eight micromachined capacitors were electrically paired (bottom electrodes connected). As described in part B, two capacitors connected in series provide the basis for force measurement. For this first design, springs were at each of the four corners of the top plate and resembled frog legs (Fig. 4). This design had been the one previously used for magnetization measurements. The motivation for the next two designs came from trying to eliminate torque response. These designs had straight springs attached to the middle of each side, resembling crossbeams (Fig. 5). The two crossbeam designs differed in their bottom plate electrode design. While one used an electrode equal in area to the top plate, the other divided the bottom plate into two electrodes. The single electrode crossbeam

capacitors came four to a chip and were paired like the frog leg devices. The double electrode crossbeam devices came four to a chip but were electrically isolated. These double electrode devices would later be paired with an external fixed capacitor during testing.

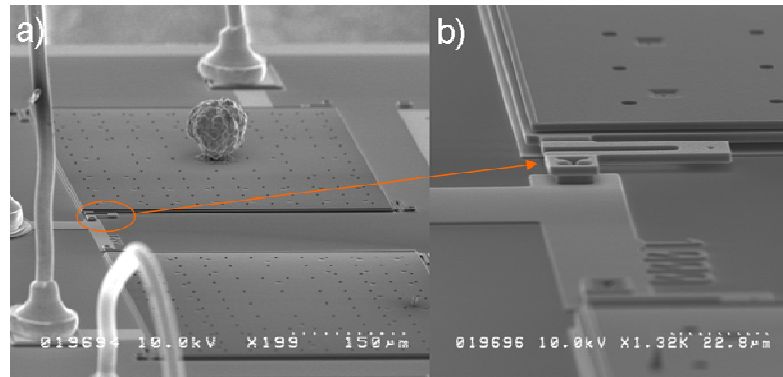


Fig. 4. (a) Springs are attached at corners of top plate. (b) Each spring resembles a frog leg.

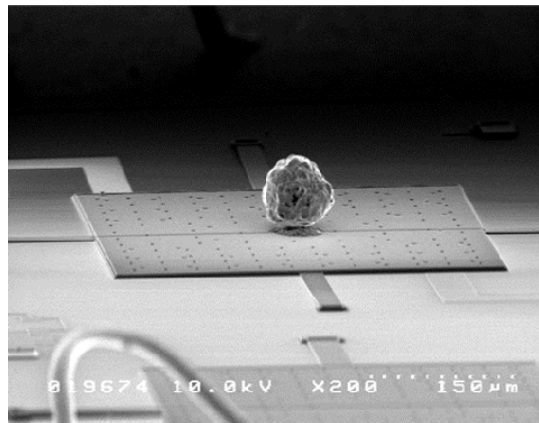


Fig. 5. Crossbeam springs.

## B. Calibration

A potential difference between the two plates generates an electrostatic force

$$F_{el} = \frac{1}{2} \frac{dC}{dx} V^2 = \frac{\epsilon_o A}{2(g_o - x)^2} V^2$$

between them. Here  $A$  is the area of the plate,  $x$  is the

plate displacement,  $V$  is the applied DC voltage,  $g_o$  is the gap for zero applied DC

voltage, and  $\epsilon_0$  is the permittivity of free space. Before magnetization measurement, the electrostatic force is used to calibrate the device. During magnetization measurement, the electrostatic force is removed and the magnetic force alone causes plate displacement. The electrostatic force is balanced by the spring force  $F_s = kx$ . The system is in static equilibrium until a critical DC voltage is applied. At this critical DC voltage, pull-in of the top plate occurs. For this reason, the top plate includes an array of small dimples on its underside, preventing it from collapsing on the fixed plate.

During magnetization measurement, the testing mechanism resembles a differential capacitor. The aim is to determine the gap displacement for a capacitor because this leads to magnetic moment calculation. Senturia [2] illustrates how differential capacitors can be used for position sensing. Two capacitors are connected in series. Each capacitor is excited by AC voltage with equal amplitude and  $180^\circ$  phase difference. If the two capacitances are the same, the output between the capacitors is zero. The output signal changes when one of the capacitors is varied while one remains fixed. As described in part A, some of the designs have two capacitors already connected. For the fixed capacitor, we either use the second micromachined capacitor or an external fixed capacitor. This measurement circuitry is depicted in Fig. 6.

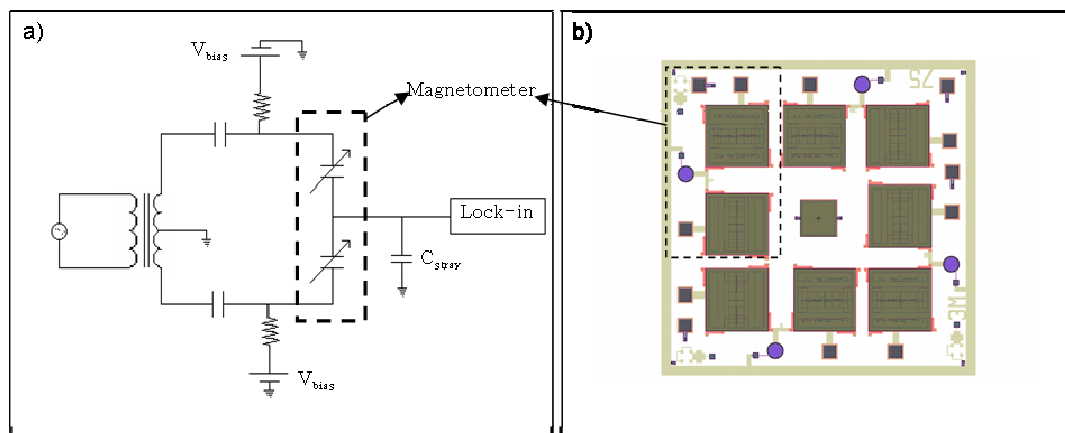


Fig. 6. (a) Measurement circuitry, and (b) design of a chip containing four magnetometers [1].

We tested this process in the lab, again with an electrostatic force from an applied DC voltage. The first step was to confirm that the devices responded well to the applied electrostatic force. In particular, we wanted to confirm that the electrostatic force between the plates varied with the square of the applied DC voltage. Fig. 7 gives electrostatic force as a function of DC voltage for some devices. Here we convert the output voltage from the differential capacitor setup to electrostatic force. This is done by dividing the predicted electrostatic force curve by the observed output voltage of the test circuit to obtain a conversion factor. This conversion factor would be different for each device (Fig. 8).

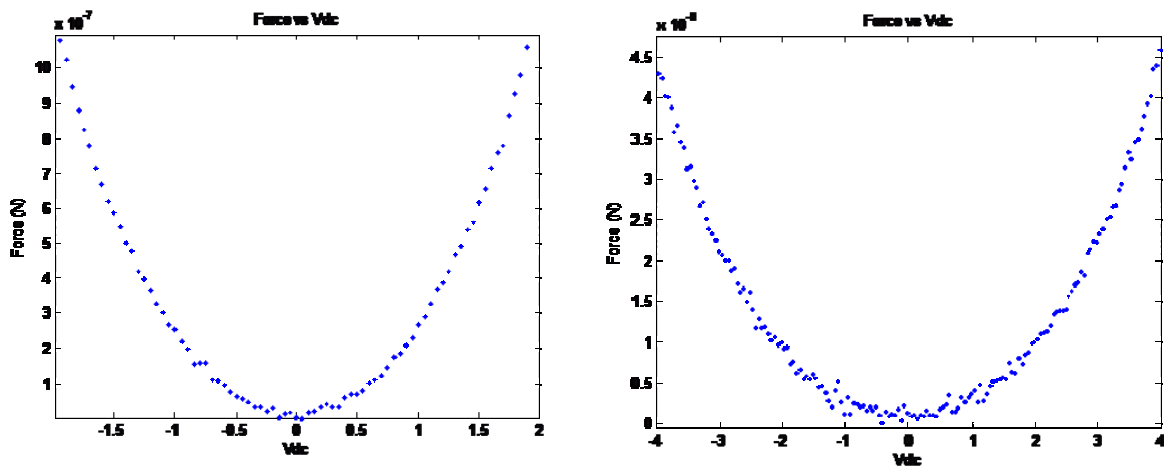


Fig. 7. Electrostatic force as a function of  $V_{DC}$  for two devices.

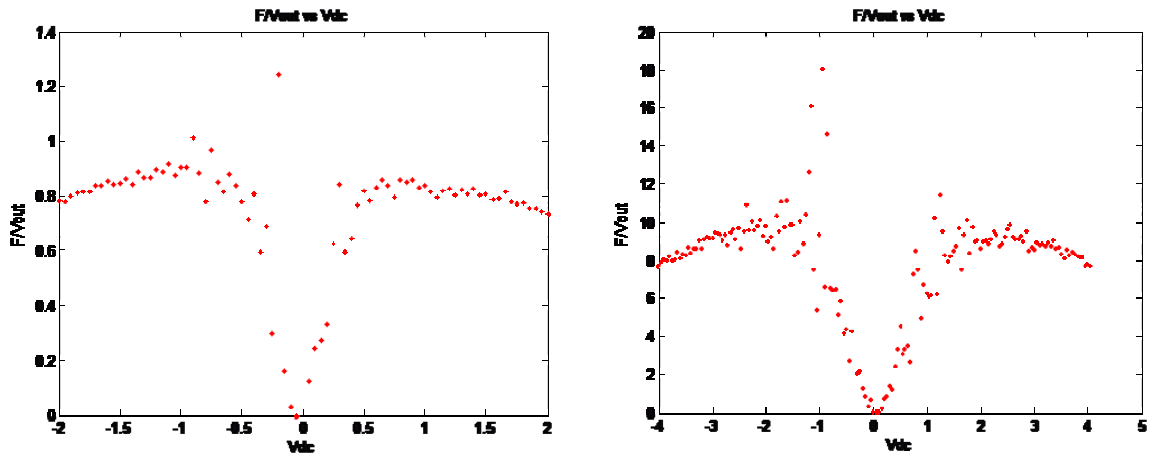


Fig. 8. Conversion factors for two devices: (a)  $\sim 0.9$  (b)  $\sim 9$ .

## IV. Discussion

After testing many of the devices, we have confirmed that the crossbeam design permits plate deformation. One reason for the deformation is that the boundary condition where the plate meets the spring causes the plate to buckle when it is displaced. In-plane compressive stress could also contribute to plate deformation. This stress might be a residual consequence of the fabrication process. The thin films of polysilicon are deposited using LPCVD, a process requiring high temperatures ( $\sim 600^\circ\text{C}$ ) [4]. During the deposition, constituent particles adhere to the substrate and tend to be separated from each other by an equilibrium distance. This distance corresponds to the lowest energy state of the system and is associated with the film being in a state with minimal stress. However, it is common that the resulting films are under considerable stress because LPCVD permits limited stress tuneability. Upon compressive stress, the constituent particles are closer together and at a higher energy level. They prefer the lower energy level and try to separate from each other [5] (Fig. 9). The fabrication of our devices introduces a sacrificial layer between the film and the substrate. When we etch the sacrificial layer, the film is suspended and free to deform under residual stress. Those films deposited with residual compressive stress buckle as the constituent particles relax and return to their equilibrium separation [5].

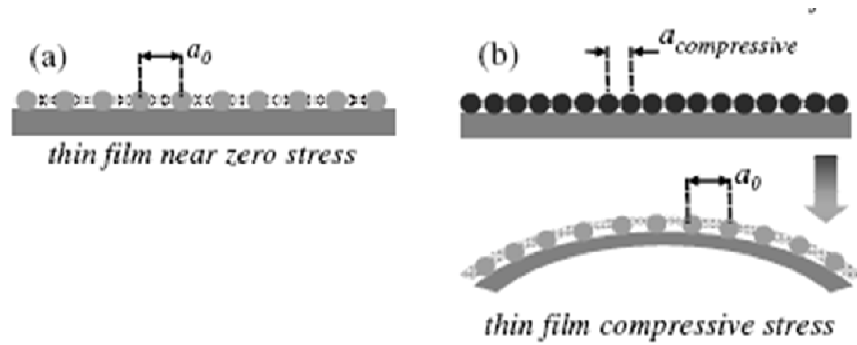


Fig. 9. (a) Constituent particles deposited at equilibrium distance  $a_0$ .  
 (b) When compressed to distance  $a_{compressive}$ , particles prefer  $a_0$  and substrate buckles. [5]

We produced a likeness of our devices using an optical profiling system. Fig. 10 is a vertical profile of a device. The image is a cross-section through the middle of the top plate and two springs. This image demonstrates plate deformation and is typical for the crossbeam spring design.

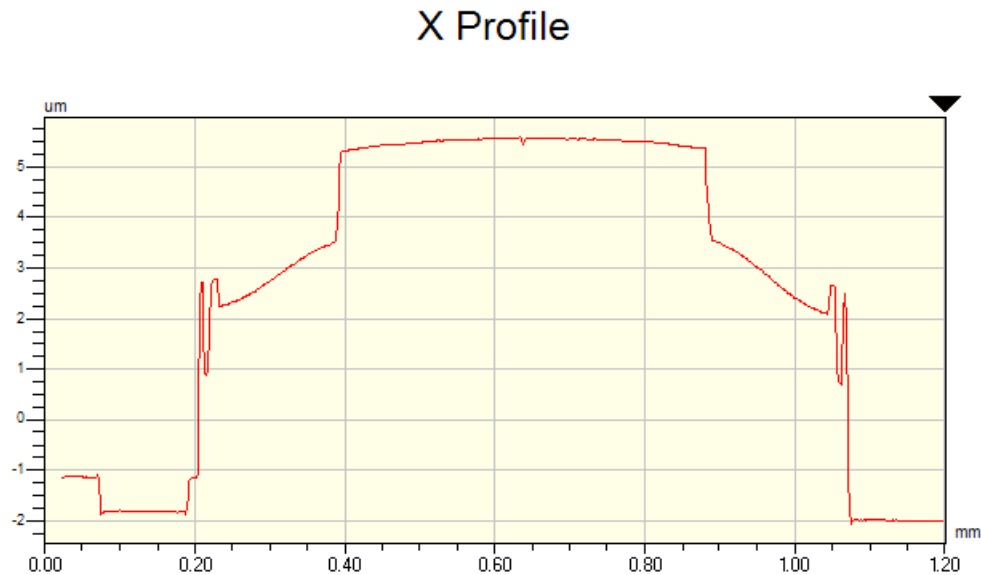


Fig. 10. Optical profile of a device.

## **V. Simulation**

COMSOL uses the finite element method (FEM) to simulate physical problems. The program reduces a given structure into a finite number of points (a process called meshing) and solves physics equations at these points. Its Multiphysics platform allows for simultaneous consideration of several physics phenomena. We needed the program to simulate electrostatics and structural mechanics, account for the moving mesh associated with deformation, and have an affinity for MEMS structures.

We incorporated the COMSOL Multiphysics software with two goals. We wanted to input the crossbeam spring design and simulate the conditions of the experiment. While the crossbeam design successfully reduced the torque response, it permitted deformation in the top plate. We wanted to know why this happened. With this information we could then move forward and simulate new designs with improved characteristics.

Before solving a problem, it is a simple task to specify the initial parameters of the system. A structure is separated into boundaries and subdomains and it is up to the user to assign physical properties to particular areas. For instance, our magnetometers are made of polysilicon. Specifying this in the program gives information such as elasticity and electrical and thermal conductivity. Indeed, for each physical incident considered in a problem (i.e., electrostatics and structural mechanics), the user must provide information about the system.

Fig. 11a shows the simplified crossbeam design as constructed in the COMSOL graphical user interface (GUI). The structure was simplified to the extent allowed while

keeping significant characteristics. This made the solution process easier. In Fig. 11b, a 10 Pa load is evenly distributed across the top plate. The color scale depicts the stress.

The plate deformation is especially apparent in the inset of Fig. 11b.

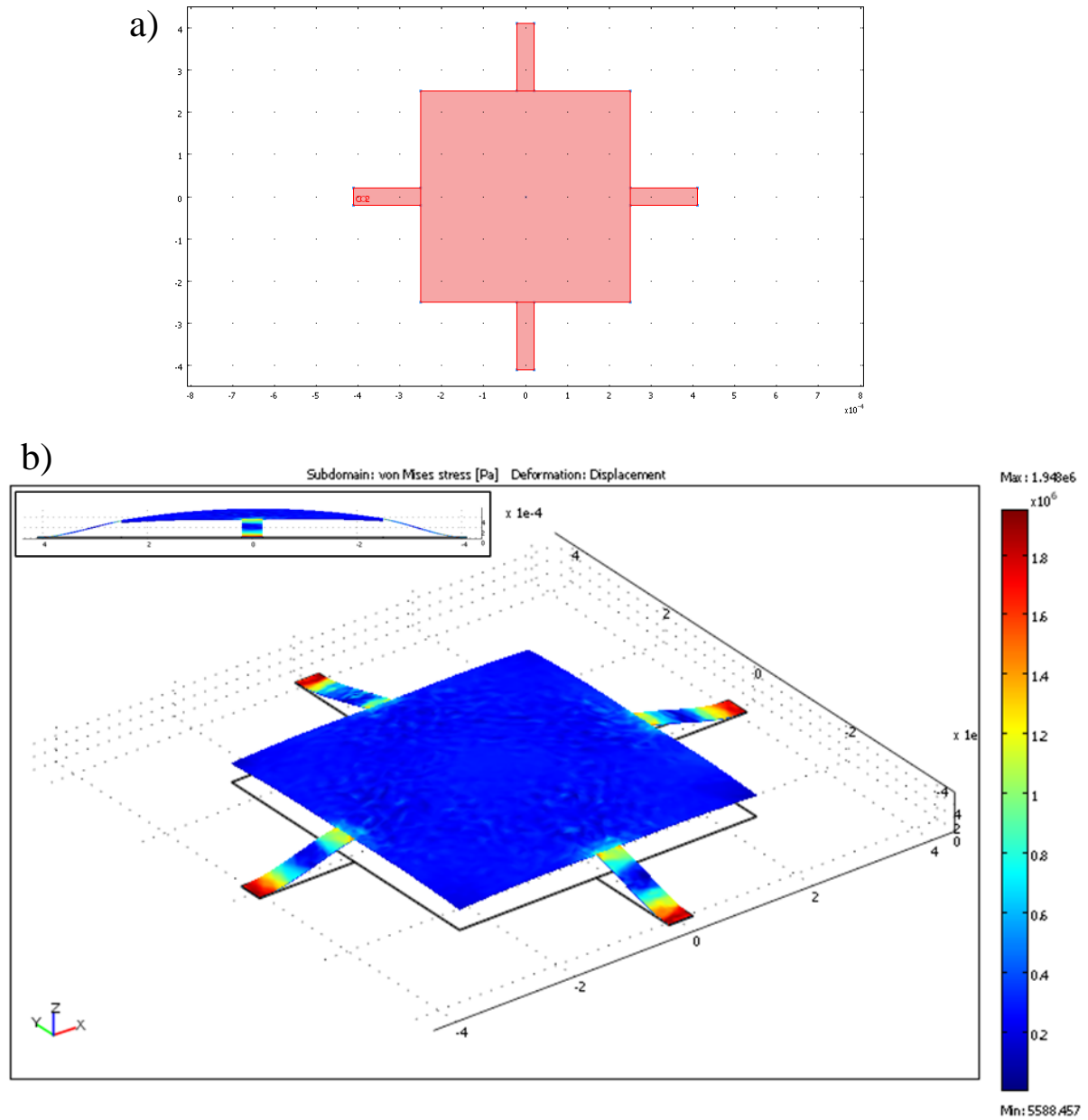
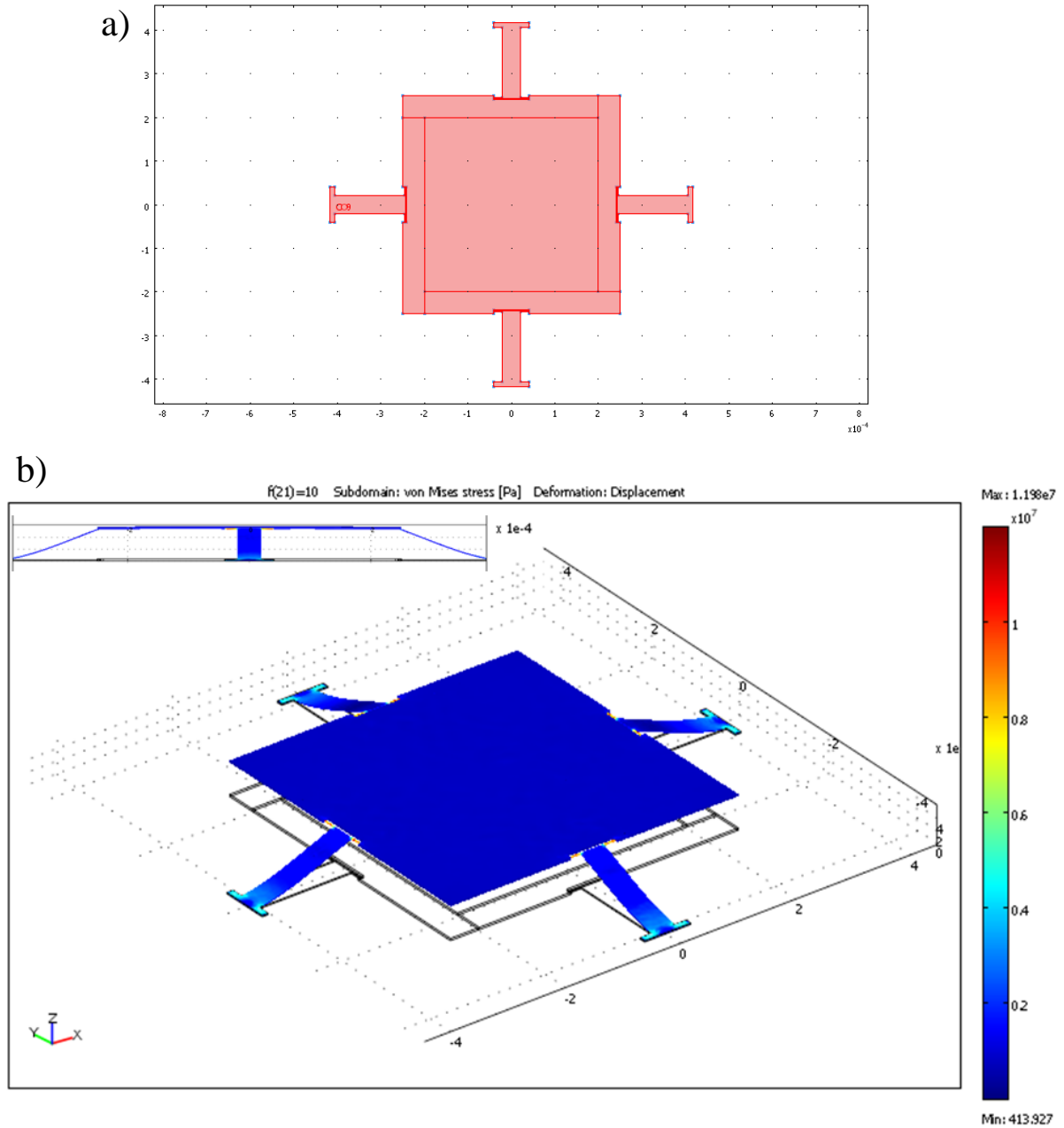


Fig. 11. (a) Simplified crossbeam design. (b) Crossbeam device undergoes 10 Pa load and deforms. Inset: View of device in xz-plane.

Meanwhile, a different spring design greatly reduces plate deformation. Fig. 12 demonstrates how a new crossbeam design reduces deformation due to boundary conditions. The rods at the plate-spring interface endure most of the stress (Fig. 12c). The inset of Fig. 12b shows the improvement.



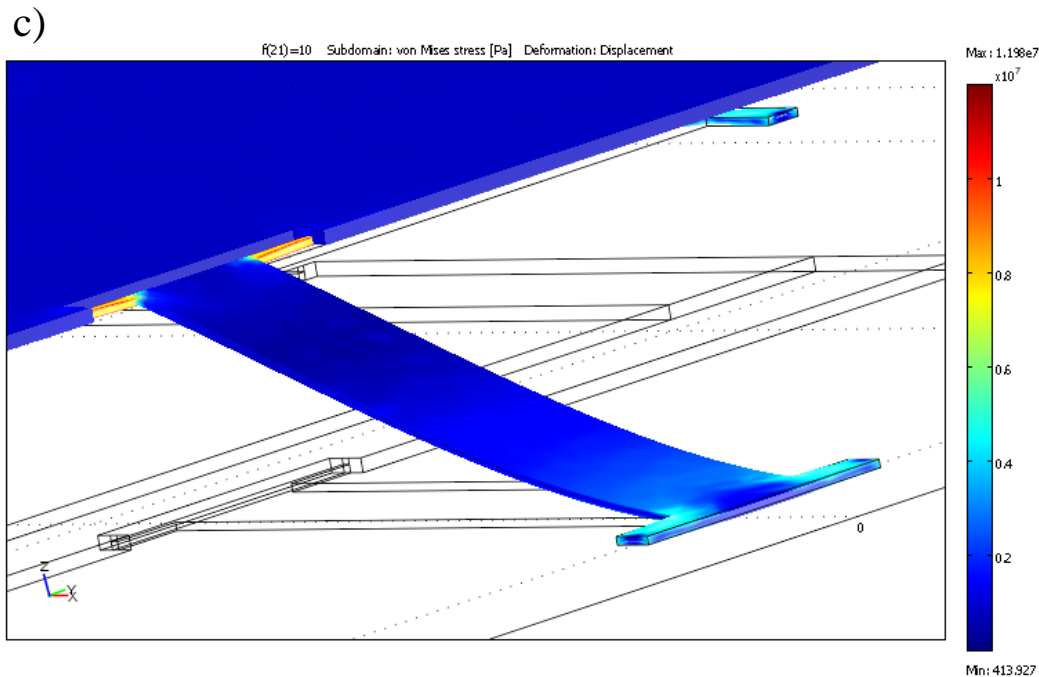


Fig. 12. (a) Simplified rod design. (b) Rod device undergoes 10 Pa load. Inset: View of device in xz-plane. (c) Spring from rod design.

## VI. Future plans and Conclusions

The COMSOL Multiphysics program has already provided significant insight into existing magnetometer designs. With the scope of the COMSOL software just being realized, simulation for our devices has only begun. Soon torque, compressive stress, and capacitance measurement will all be utilized with the program. We believe that this software can be used to simulate properties for novel device designs and will forward the development of MEMS magnetometers.

## VII. Acknowledgments

I thank my mentors Ho Bun Chan and Konstantinos Ninios. I am grateful to have participated in their research. Also, thank you to Kevin Ingersent, Selman Hershfield, and Kristin Nichola who have made this REU program successful. Finally, thank you to the National Science Foundation for providing all of us with funding.

## References

- [1] K. Ninios, graduate qualifying report, University of Florida, Gainesville, FL, 2008 (unpublished).
- [2] Senturia, Stephen, *Microsystem Design*, (Springer Science and Business Media, Inc., New York, 2001).
- [3] David Koester, Allen Cowen, Ramaswamy Mahadevan, Mark Stonefield, and Busbee Hardy, *PolyMUMPS Design Handbook*, 2 (2003).
- [4] R.C. Teixeira, I. Doi, M.B.P. Zakia, J.A. Diniz, and J.W. Swart, *Materials Science and Engineering B* **112**, 160-164 (2004).
- [5] **M. Martyniuk**, J. Antoszewski, C.A. Musca, J.M. Dell, and L. Faraone, *Smart Mater. Struct.* **15**, S29–S38 (2006).